# Excitation-Tunable Tip-Enhanced Raman Spectroscopy

Niclas S. Mueller,[†] Sabrina Juergensen,[†] Katja Höflich,[‡] Stephanie Reich,[†] and Patryk Kusch*,[†]

[†]Freie Universität Berlin, 14195 Berlin, Germany

[‡]Helmholtz-Zentrum Berlin für Materialien und Energie GmbH, 14019 Berlin, Germany

S *Supporting Information*

ABSTRACT: Tip-enhanced Raman spectroscopy (TERS) is a powerful tool to investigate chemical composition, for obtaining molecular information and for recording images with a spatial resolution on the nanometer scale. However, it typically has been limited to a fixed excitation wavelength. We demonstrate excitation-dependent hyperspectral imaging by implementing a wavelength-tunable laser to our TERS setup. Varying the excitation wavelength during the TERS experiments is a key to perform spatially resolved resonant Raman scattering with nanometer resolution, which enables mapping of transition centers and to study, for example, the quantum properties of electrons and phonons. To present the application potential and to verify the setup, we recorded excitation-dependent hyperspectral nanoimages of a densely packed film of carbon nanotubes (CNTs) on an Au surface and use the spectral position and intensity of the radial breathing modes for a unique assignment of the CNTs. We succeeded in identifying and imaging at least nine different tube species. The nanoimages revealed the exact position and the distribution of certain CNTs inside the film. e-TERS will have manifold application in nanoimaging, for chemical analysis, and electronic studies on the nanometer scale, making it highly interesting in fields ranging from biomedicine and chemistry to material science.
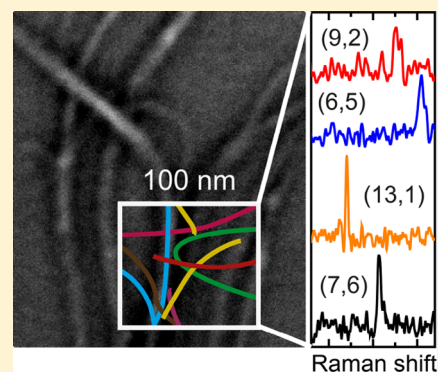
INTRODUCTION

Imaging far below the diffraction limit of light is of critical importance in many scientific disciplines, as it enables the visualization of assemblies of nanoobjects such as individual nanotubes, nanowires, viruses, bacteria, DNA, and even single molecules.[1−8] A powerful technique for optical nanoimaging is tip-enhanced Raman spectroscopy (TERS) that is moreover fingerprint-type and label-free.[9−13] TERS routinely provides information on the topography and chemical composition, together with optical images, with a spatial resolution of a few nanometers.[14−17] Prominent examples for nanoimaging and chemical analysis by TERS include the visualization of single carbon nanotubes (CNT's), defects in graphene, and single strands of RNA, making TERS an invaluable tool in chemistry, biology, and physics among others.[10,18−23]

TERS is based on the illumination of a sharp metallic atomic force microscope (AFM) or scanning tunnel microscope tip with light and recording simultaneously Raman spectra.[24−26] The incoming light excites localized surface plasmons (LSPs) in the tip and often also in the substrate.[27−30] The LSPs generate a strongly localized electromagnetic (EM) field (near-field),[10,18,21,31] which has two functions in TERS. First, it locally enhances the incoming and the Raman scattered light by several orders of magnitude. Second, it is spatially restricted to a few nanometers and leads to a localized excitation of the sample. By recording tip-enhanced Raman spectra, and plotting their intensity as a function of tip position, TERS enables nanoimaging with a spatial resolution below 10 nm.[6,17,25] The absolute enhancement in TERS and its

sensitivity strongly depends on the morphology and material composition of the exciting tip.[27,32] By changing the material or the geometry of the tip, it is possible to tailor the EM near-field and maximize the sensitivity of TERS.[27,33] Optimized TERS setups may exhibit an enhancement of 10^{11} in the intensity of the Raman signal, enabling the investigation and visualization of single molecules.[15,25,29,34]

Despite the great success of TERS for nanoimaging, common TERS experiments were performed at, and optimized for, one particular excitation wavelength.[14,25,35] This guarantees extremely high enhancement of the Raman intensity and a huge sensitivity.[32,33] The major drawback is that fixed single line excitation prevents performing excitation-dependent TERS. Tuning the excitation wavelength during TERS will enable spatially resolved resonant Raman scattering (RRS) and a mapping of the electronic and optical transitions of samples with a lateral resolution down to few nanometers.[36−40] This will allow the nanoimaging of optical transition energies and will give in addition to the chemical and vibrational information obtained by TERS also insight into the optical properties of a variety of samples.

Here, we introduce excitation tunable TERS (e-TERS), an advanced technique that extends TERS with tunable excitation by applying a continuously tunable laser source. In e-TERS, hyperspectral TERS maps are recorded for the same area on

the sample with various excitation wavelengths. To enable the tunable excitation, we equipped our TERS setup with a fully tunable optic parametric oscillation (OPO) laser (spectral coverage of 450−650 nm in the visible). As a first application and for validating e-TERS, we obtain excitation energy-dependent nanoimages of a large film of CNTs on a gold surface. By recording spatial maps of the tip-enhanced radial breathing modes (RBMs) at different excitation wavelengths, we demonstrate nanoimaging and the unique assignment of different CNT species inside the film, in which the tubes are randomly distributed. We obtain hyperspectral nanoimages of nine different CNT species in a 100 nm × 100 nm area. Additionally, we record a large high-resolution hyperspectral nanoimage of a (7,5) tube that is located inside a 2 μm × 2 μm sample area and has a length of approximately 1 μm. We used PtIr-coated tips for the e-TERS experiments in gap mode TERS configuration and demonstrate experimentally that they guarantee tip-enhancement for a broad spectral excitation region ranging from 532 to 650 nm. We support this observation by numerical simulations of the field enhancement generated by the metallic tip.

■ METHODS

Similar to conventional TERS setups, our e-TERS setup consists of three parts (Figure 1): an atomic force microscope,
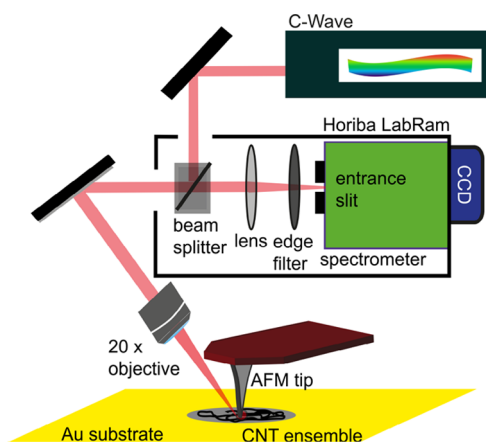
Figure 1. Scheme of the hyperspectral TERS setup. As a source of excitation energy, a fully tunable OPO laser is connected to a HORIBA LabRAM Raman spectrometer. The laser beam is guided through a beam splitter and focused by a 20× objective onto the tip apex of an AFM probe. The backscattered light is again collected by the objective. Raman spectra are recorded by guiding the tip-enhanced Raman scattered light of the sample via an edge filter into a grating spectrometer.

Raman spectrometer, and laser excitation source. As a basis for the e-TERS, we used a Park scientific AFM and a HORIBA Jobin Yvon LabRAM HR500 spectrometer, operating in side illumination mode and equipped with a 633 nm HeNe laser and a 600 gr/mm grating. In the setup, the laser light is guided to a beam splitter and is reflected to the HORIBA TERS extension, which is coupled to the Park AFM. A 20× objective focuses the beam onto the AFM tip and collects the backscattered light. The backscattered light is guided through the beam splitter. To suppress Rayleigh scattering and to be able to vary the excitation wavelength, we replaced the 633 nm single line notch filter of the LabRAM by an exchangeable edge

filter. A lens focuses the light into the spectrometer and finally on an Andor iDUS 416 Si charged coupled device.

To realize the e-TERS setup, we replaced the HeNe with a C-WAVE laser (Hübner Photonics), that is, a continuous-wave, wavelength-tunable OPO laser as shown in Figure 1. The excitation wavelength provided by the C-WAVE laser can be tuned quasi continuously from 450 to 650 nm in the visible and from 900 to 1300 nm in the infrared (IR) excitation region. The main advantage of the C-WAVE compared with many other wavelength-tunable systems is the pointing stability of the laser beam; after changing the excitation wavelength, the position of the laser spot remained constant on the tip. No realignment of the beam path was required. The laser had to be refocused slightly only by the 20× objective allowing for fast measurements at multiple wavelengths.

We chose to work in noncontact (i.e., tapping) mode, where the tip oscillates at its mechanical resonance frequency. The noncontact mode leads to lower tip-enhancement compared with the contact mode,[26] resulting in lower Raman intensity during the TERS experiments, but avoids distortion of the samples. Conventional TERS setups work in contact mode leading to very high enhancement (up to 10^{10}),[15,41] but at the great risk of distorting, manipulating, or even destroying the sample by the AFM tip.[42−44] For example, we found that we moved CNTs and picked them up when working in contact mode. We also decided to use gap mode TERS, where the metallic tip is located above a gold substrate, yielding to higher enhancement factors.[34]

During all TERS experiments, we kept the laser power at 300 μW. To record nanoimages, we first record a 2 × 2 μm^2 topography image of the sample by the Park AFM. We chose a 100 × 100 nm^2 area inside the topography that is close to distinctive points (scratches or holes) and thus could be easily recognized. Inside the probing area, we measured at each position of the tip a TER spectrum. For each TER spectrum, the acquisition time was 3 s. The distance between two tip positions, where we recorded a TER spectrum, was 10 nm in x and y direction. After changing the excitation energy, we again recorded a 2 × 2 μm^2 topography image and identified the probing area. This allowed us to minimize effects of sample drift and to ensure that the nanoimages belong to the same probing area. Furthermore, we recorded a large nanoimage with a size of 0.55 × 0.14 μm^2. The distance between two tip positions was 5 nm. The acquisition time was kept at 3 s. The nanoimages presented in Figures 4, 5 and 6 show the TER intensity as a function of tip position in color fill contour plots. The intensity pixel images (where each pixel corresponds to one particular tip position and one TER intensity) can be found in the Supporting Information (Figures S5 and S6).

For the experiments, we used commercially available single-wall CNTs from SouthWest Nanotechnologies (batch no. 76), which were produced by a CoMoCat catalytic CVD process. The CNTs are dispersed in an aqueous solution with an initial nanotube concentration of 0.1 g/L. For unbundling the tubes, 1 wt % sodium dodecyl sulfate was added and the solution was tip-sonicated at 50 W for 1 h, followed by a 1 h centrifugation at 31 000g and 25 °C. The supernatant was dropped onto a commercial available gold substrate from Georg Albert PVD−Beschichtungen. The solution comprises a wide variety of different tube species, with varying diameters. After water evaporation, the CNTs form a large-volume film of CoMoCats randomly distributed over the Au substrate (Figure 3b).

Before the tubes were brought onto the Au surface, we characterized the CNT solution by photoluminescence excitation (PLE) spectroscopy. The PLE experiments were done with a HORIBA Jobin Yvon Fluorolog-3 spectrofluorometer, equipped with an InGaAs detector (Symphony, HORIBA). Using PLE, we identified which CNTs are in the solution by plotting the second optical transition of the CNTs (excitation energy) versus the first transition energy (emission energy).[45] The resulting PLE map is shown in Figure 3a. From the map, we determined several emission maxima at particular excitation wavelengths. By comparing the appearing maxima with literature,[45,46] we identified at least 13 different semiconducting tubes, which are marked in Figure 3a. We can also estimate the optical transition wavelength of certain tube species from the excitation wavelength in the PLE map.

Scanning electron microscopy (SEM) was performed using a Zeiss Merlin KMAT microscope equipped with a Gemini II column that allows for high-performance imaging at low acceleration voltages. In our case, an acceleration voltage of only 600 V was required to resolve the nanometer sized topography of the CNT and to avoid distortions in the images. A small imaging current of 70 pA was used to minimize the electron beam spot size. To achieve a sufficient signal-to-noise ratio under these beam conditions, the working distance was set to 1.8 mm using the InLens detector for image acquisition. The diameters of the single-walled CNT are at the detection limit of SEM. While CNTs with diameters above 5 nm could be well resolved, CNTs of smaller diameters cannot be safely identified as they merge with the background signal. Hence, in contrast to the e-TERS technique that works independently from the CNT topography, a significant amount of CNTs remains invisible in SEM imaging.

The finite-difference time-domain simulations were conducted with the commercial software package, Lumerical FDTD Solutions. The simulation setup is similar to that in our previous work.[26] The tip was modeled as a Si cone with a 5 nm apex radius and 32° cone angle, coated with a 25 nm thick layer of Pt or Au. We neglected the Ir in the simulations, as the coating of the PtIr tip consisted of 95% Pt and only 5% Ir. The materials were modeled by fitting experimental data of the dielectric functions from ref 47 for Au and from ref 48 for Pt and Si.[47,48] Adaptive meshing was used to discretize the space close to the tip and substrate with a 0.5 nm cell diameter in the gap. The distance between the tip and gold surface was 4 nm. The tip was illuminated by a p-polarized plane wave at an incidence angle of 30° relative to the gold surface. The field enhancement was calculated as the absolute value of the local electric field amplitude normalized to the incident electric field amplitude at a position in the center of the gap between tip and substrate.

RESULTS AND DISCUSSIONS

A main challenge for e-TERS was to find a tip that allows exciting a near-field between the tip and substrate for a broad spectral excitation range in the visible.[10,18,30,49] Realizing e-TERS is impossible if the tip has to be replaced after a change of the excitation wavelength. We suggest that PtIr-coated AFM tips are excellent candidates for e-TERS. As demonstrated in our previous work,[26] in gap mode configuration with an Au substrate (Figure 2a), PtIr-coated AFM tips provide excellent TERS enhancement. We calculated the excitation wavelength-dependent field enhancement defined as the ratio between the maximum near-field amplitude and illuminating field amplitude
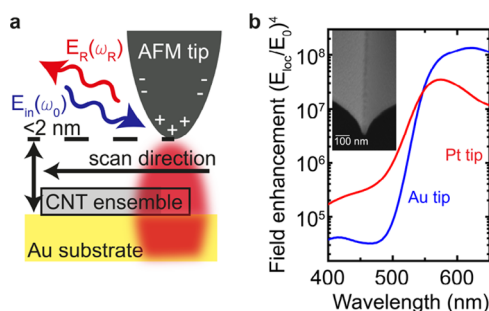
Figure 2. (a) Principle of e-TERS. The incoming laser light illuminates the metallic tip and excites a near-field between tip and substrate. The strongly localized near-field drives the Raman process, that is, it stimulates the sample and enhances the incoming and Raman scattered light. (b) Finite-difference time-domain simulation of the wavelength-dependent field enhancement $(E_{loc}/E_0)^4$ between a PtIr-coated tip (red) and an Au tip (blue) above an Au substrate with 4 nm distance. The inset in (b) shows a SEM image of the apex of the PtIr-coated tip. A high-resolution image is provided in the Supporting Information (Figures S7 and S8).

E_{max}/E_{in} using FDTD simulations. The intensity of the tip-enhanced Raman scattered light scales with the fourth power of the field enhancement.[34] The calculated profile in Figure 2b (red curve) demonstrates that the PtIr-coated AFM tip provides field enhancement over a broad wavelength range from 510 to 650 nm. We also calculated the field enhancement profile of a Au tip above a Au substrate. Indeed, the Au tip yields higher peak enhancement, its wavelength-dependent range shown in Figure 2b (blue curve) is narrower. This finding is in nice agreement with the enhancement provided by an Au nanosphere dimer with a 4 nm gap size.[50] For wavelengths below 550 nm, the Pt tip yields larger field enhancement than the Au tip. We support this finding by experimental observations: during the experiments, we were never able to realize TERS by using Au tips and an excitation wavelength below 550 nm (see Supporting Information Figure S4). Au tips are to be used for highest field enhancement, for example, for single molecule detection. In contrast, PtIr-coated tips are the optimum choice for e-TERS experiments, where the excitation wavelength is varied over a broad spectral range.

To demonstrate the performance of e-TERS, we used the setup in Figure 1 to characterize and nanoimage the transition energies of an ensemble of CNTs placed on an Au substrate. We selected CNT films as an ideal test bed to map optical transitions and local vibrations via resonant e-TERS. The film is formed by CNTs of different species (chiralities) with varying electronic, optical, and vibrational properties.[51] The chirality of a CNT is characterized by the tuple (n,m) that quantifies the graphene lattice vector $c = n \cdot a_1 + m \cdot a_2$ around the CNT circumference CNT,[51,52] a_1 and a_2 form the unit cell of graphene. Some CNTs are metallic, others have a band gap in the IR and visible. In PLE experiments (see Methods), we identify at least 13 different semiconducting tube species with different optical transitions which are marked by their chiral indices in the PLE map in Figure 3a. Suspended CNTs were dropped on an Au substrate where they formed a closed film. It consisted of randomly aligned and distributed CNTs and CNT bundles. An exemplary SEM image of the sample is shown in Figure 3b. In contrast to spectroscopy techniques, SEM can only visualize objects of sufficiently large sizes. In our case, only bundles of CNTs and separated CNTs with diameters larger than 5 nm may be identified.
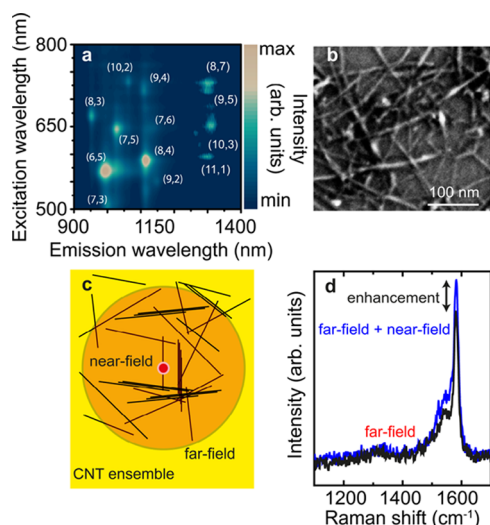
Figure 3. (a) PLE map of CNTs dispersed in an aqueous solution. The CNT species are indicated by the chiral indices. (b) Exemplary SEM image of the CNTs placed on an Au surface, (c) scheme of the CNT ensemble that is stimulated by the near-field generated between tip and substrate (red dot) and the excitation laser (large red circle). (d) Composed near- (blue) and far-field Raman spectrum (black) of the characteristic G band of the CNTs.

In resonant e-TERS, we want to combine the nanometer spatial resolution of TERS and the possibility to determine optical transition of RRS. RRS is a well-established tool to identify particular CNT species that are present in a CNT ensemble. For a unique assignment of the CNTs in RRS, the fingerprint-type RBMs of particular CNTs are recorded at different excitation wavelengths.[46,53,54] The RBMs are only excited when the incoming light matches the optical transition of the CNTs, that is, if the excitation wavelength is in resonance with an optical transition of a particular chirality. The RBM modes appear in the Raman spectrum in the low-frequency range between 150 and 350 cm^{-1}.[54,55] Different tube species have different optical transition energies. By knowing the excitation wavelength and the frequency of the RBM, we are able to assign a CNT species that is present inside an ensemble or a film.[40,46,52,54,55] Conventional RRS is restricted to the diffraction limit of light. Resonant e-TERS overcomes this limit and will enable nanoimaging of CNTs, mapping of their optical transitions, and allow a unique assignment of chiralities on the level of an individual CNT.

For the alignment of the e-TERS setup, we approached the PtIr-coated tip to the CNT film and recorded a Raman spectrum of the G band, see Figure 3d blue line. The spectrum is composed of the tip-enhanced Raman (TER) spectrum belonging to the volume stimulated by the EM near-field (red dot in Figure 3c) and the conventional Raman scattering from all illuminated CNTs (Figure 3c large orange disk). The TER spectrum originates typically from an area of a few nanometers, depending only on the size of the EM near-field hot spot generated between tip and substrate.[18] As can be seen in the sketch in Figure 3c, the scattering volume of the conventional Raman signal is orders of magnitude larger than the scattering volume excited by the EM near-field generated at the tip apex and will dominate the total Raman signal. To verify that tip-enhanced Raman scattering is realized, we retracted the tip and, again, recorded a spectrum with decreased intensity (Figure 3d black spectrum).

After optimizing the TER intensity, we used the AFM to take the topography image in Figure 4a. The topography image
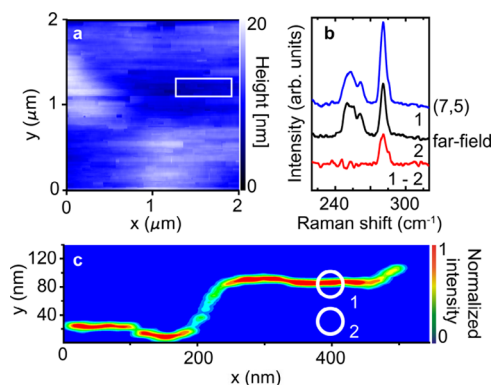

Figure 4. (a) Topography image of a 2 × 2 μm CNT film. The position of the (7,5) in panel (c) is indicated by the white box. (b) Composed (blue), far-field (black) and TER spectra (red) of RBMs of the (10,3), (7,6), and (7,5) species. (c) Nanoimage of the (7,5) CNT, obtained by plotting the tip enhanced RBM intensity as a function of tip position.

provides no information on the distribution of CNTs in the film because the film is densely packed and the tip apex is too large to visualize single CNTs inside the film. We will now demonstrate how to visualize CNTs in the film via e-TERS. We start with 633 nm excitation. It is in resonance with (7,5), (7,6), and (10,3) CNTs.

To image particular CNT species by applying resonant e-TERS, first a composed Raman spectrum of the RBM is recorded by placing the PtIr-coated tip at a particular position above the CNT film. The resulting spectrum in Figure 4b (blue) consists of the RBM peaks of the (10,3), (7,6), and (7,5) CNTs.[52,54,55] We retracted the tip and recorded a Raman spectrum (Figure 4b, black) without the TER contribution to the signal (far-field spectrum). The (7,5) RBM mode decreased in intensity with the retraction of the tip, whereas the (7,6) and (10,3) RBMs remained unchanged. Subtracting the far-field spectrum from the composed spectrum, we obtained the pure TER spectrum, see Figure 4b (red). From the TER spectrum, we identify the tube species that is located below the tip as the (7,5) CNT. To map the (7,5) CNT with the e-TERS, we repeat the procedure as a function of (x,y) tip position and determined the TER (7,5) intensity. In Figure 4c, we show the exact position of the (7,5) CNT in a 2 × 2 μm^2 area consisting of randomly distributed CNTs. The (7,5) CNT is around 800 nm long and is bent in a step-like shape in the (x,y) plane.

In the far-field Raman spectrum shown in Figure 4b, we observed besides the (7,5) RBM two more RBMs belonging to the (7,6) and (10,3) CNTs (Figure 5a). In a second run, we scan another area of the CNT film with a size of a 100 nm × 100 nm with the e-TERS with a step size of 10 nm in x and y. We obtained, in the same way as described above, the TER RBM spectra of the (7,5), (7,6), and (10,3) CNTs to image them (Figure 5b). In Figure 5c, we show an image of the (7,6) CNT by plotting its TER RBM intensity as a function of the tip position. We repeated this for the other two RBMs and nanoimaged the (7,5) and (10,3) CNTs. By overlapping the (7,5), (7,6), and (10,3) nanoimages, we identify their combined positions in the scanning area. As can be seen in Figure 7d, the (7,5) tube lies in the middle of the area. The
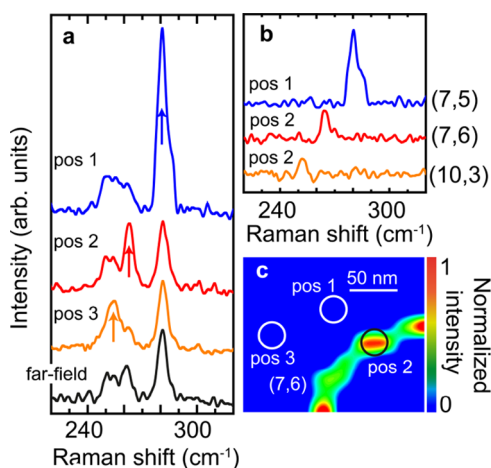
Figure 5. (a) Composed spectra recorded at three different positions of the AFM tip. (b) Pure TER spectra of three different RBMs, obtained by subtracting the far-field spectrum from the composed spectra. The tube species were assigned by the Raman shift of the appearing RBM. (c) Nanoimage of the (7,6) CNT.

(7,6) tube is strongly bent and meets the (7,5) CNT at the bottom part of Figure 7d. The (10,3) CNT is located on the left. Right below the (10,3) CNT, another (7,5) tube is located. Using the 633 nm excitation, we nicely visualize three CNT species.

From the PLE experiment (Figure 3a), we know that more CNT species are present in the solution and the CNT film. These tubes have different optical transition energies.

In a conventional TERS setup, it would be impossible to image and identify other CNT species, as these setups use a single excitation wavelength.[14,25,35] Our e-TERS has the huge advantage that the excitation wavelength can be varied quasi-continuously.

We now change the excitation to bring other species in resonance and nanoimage them. To continue the examination of the CNT film, we chose along with 633 nm as excitation wavelengths, 532, 568, and 600 nm, which gives us access to further tube species, see Figure 6, gray markings. For hyperspectral nanoimaging by e-TERS, we recorded again, at each position of the tip, a composed Raman spectra of the RBM and subtracted the far-field Raman spectrum. Afterward, we fitted the TER spectrum to identify the RBM intensities,
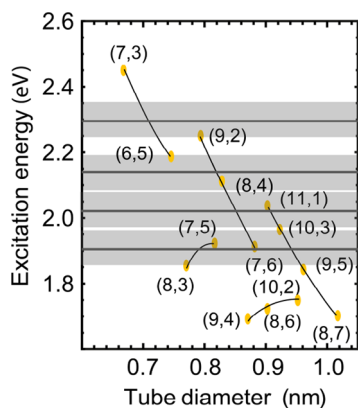

Figure 6. Kataura plot showing the excitation energy as a function of CNT diameter enabling to identify the accessible CNTs in e-TERS with the four chosen excitation wavelengths (gray markings).

which yield the hyperspectral nanoimages. We observed a total of nine CNT species and recorded their positions in the scanning area, see Table 1 and Figure 7. At 633 nm, we imaged

Table 1. Summary of All Observed RBM Frequencies and Their Assignment to CNT Species[a]

excitation (nm)	tube species	d (Å)	ω_{RBM} (cm^{-1})	E_{ii} (eV)	properties
600	(9,9)	12.1	195.3	2.020	metallic
600	(13,1)	10.60	220.3	2.057	metallic
600	(12,0)	9.40	244.9	2.180	metallic
600	(11,1)	9.03	256.0	2.031	semiconducting
532	(9,2)	7.95	288.0	2.280	semiconducting
568	(6,5)	7.47	308.6	2.180	semiconducting
633	(10,3)	9.24	252.1	1.945	semiconducting
633	(7,6)	8.83	264.2	1.909	semiconducting
633	(7,5)	8.18	283.3	1.915	semiconducting

[a]The diameter and optical transition energies of the CNTs energies are provided. They were obtained from ref 45. The CNTs are grouped in metallic and semiconducting tubes.
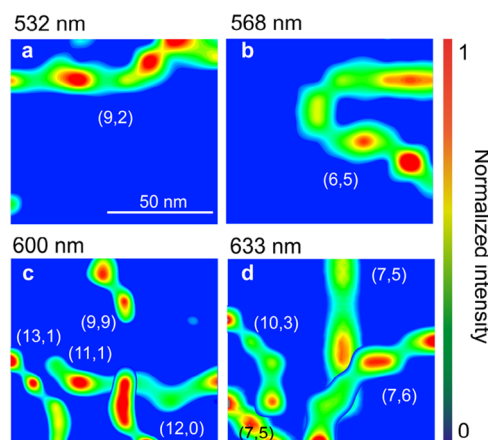
Figure 7. Nanoimages of the CNTs recorded with excitation wavelengths of (a) 532, (b) 568, (c) 600, and (d) 633 nm. The TER intensity of the RBMs is plotted as a function of tip position. The tube species were identified by their RBMs and labeled by the chiral indices in the nanoimages.

three CNT species (Figure 7d). At 568 nm, the (6,5) CNT was observed (Figure 7b). Using 600 nm wavelength, we imaged the metallic (13,1), (9,9), and (12,0) CNTs (Figure 7c), which were invisible in the PLE map and the semiconducting (11,1) CNT. The option to detect metallic and semiconducting CNTs simultaneously is unique to RRS because metallic tubes emit no luminescence. Impressively, we were also able to use the 532 nm excitation wavelength for TERS without changing the AFM tip. We obtained the hyperspectral image of the (9,2) CNT in Figure 7a. The nanoimages in Figure 7 demonstrate the ability of e-TERS to visualize the shape and orientation of different CNT species even for overlapping CNT positions.

Not every CNT species that was resonant with the exciting lasers appeared in our scanning area. From the PLE map in Figure 3a, we know that (8,4) CNTs are also present in the solution with an optical resonance energy at 590 nm. We indeed observed the RBM of the (8,4) tube in the far-field Raman spectrum at an excitation wavelength of 600 nm, but it was never present in the TER spectra (see: Supporting

Information, Figure S3). This means that (8,4) CNTs are in the CNT film but not inside the 100 nm × 100 nm probe area. This shows that we are able to find out whether a CNT is present inside the probe area and, furthermore, to estimate the CNT distribution from the TER RBM spectra as a function of excitation wavelength and tip position.

We envision manifold applications of e-TERS in various fields of science, ranging from material science, chemistry, physics, and biology. e-TERS offers the possibility to identify and image optical transitions as demonstrated on the CNT film. This opens a new possibility to study electronic and vibronic properties with nanometer spatial resolution, making e-TERS a powerful analysis tool for many materials, ranging from molecules and macromolecules to different 1D and 2D samples. By applying e-TERS, for example, on a macro-molecule, it will be possible to map its optical transition centers and localized electronic states. Furthermore, e-TERS will enable nanoimaging, nanoscale-resolved chemical and compositional analysis, and quality control. It detects and images localized chemical interactions and chemical bonds as well as defects and strain, which will be interesting for examining 2D materials.

CONCLUSION

In conclusion, we introduce a new nanoimaging tool for recording spatially resolved excitation-dependent hyperspectral images by applying a fully tunable visible laser to a TERS setup, namely, the e-TERS. By plotting the TER intensity as a function of tip position and excitation wavelength, our setup enables us to perform spatially resolved RRS with a resolution on the nanometer scale. We demonstrate the capability of e-TERS by studying an ensemble of CNTs placed on an Au surface. Using four different excitation wavelengths, we identified nine metallic and semiconducting CNTs in a 100 nm × 100 nm sample area and determine their distribution and orientation by recording hyperspectral nanoimages. We also recorded a high-resolution image of the (7,5) CNT in a 2 × 2 μm sample area following its length almost over a micron. All e-TERS experiments were conducted with PtIr-coated tips above an Au surface, which shows that these tip materials are an interesting alternative to gold and silver as commonly used in TERS. We demonstrated experimentally and by FDTD simulations that the PtIr-coated tips can be used for TERS at different excitation wavelengths in a broad spectral region of at least from 530 to 650 nm.

ASSOCIATED CONTENT

Ⓢ Supporting Information

The Supporting Information is available free of charge on the ACS Publications website at DOI: 10.1021/acs.jpcc.8b10272.

> Tip-enhanced Raman spectra of RBMs at different excitation wavelengths; e-TERS nanoimage of the (7,5) nanotube; e-TERS nanoimages recorded at different excitation wavelengths; and SEM images of the PtIr-coated AFM tip (PDF)

AUTHOR INFORMATION

Corresponding Author

*E-mail: patryk.kusch@fu-berlin.de.

ORCID Ⓞ

Niclas S. Mueller: 0000-0002-8688-1974
Katja Höflich: 0000-0003-4088-2928

Patryk Kusch: 0000-0001-9180-786X

Notes

The authors declare no competing financial interest.

REFERENCES

(1) Bustamante, C.; Vesenka, J.; Tang, C. L.; Rees, W.; Guthold, M.; Keller, R. Circular DNA Molecules Imaged in Air by Scanning Force Microscopy. *Biochemistry* **1992**, *31*, 22−26.

(2) Duday, D.; Clément, F.; Lecoq, E.; Penny, C.; Audinot, J.-N.; Belmonte, T.; Kutasi, K.; Cauchie, H.-M.; Choquet, P. Study of Reactive Oxygen or/and Nitrogen Species Binding Processes on E. Coli Bacteria with Mass Spectrometry Isotopic Nanoimaging. *Plasma Processes Polym.* **2013**, *10*, 864−879.

(3) Gilmore, J. L.; Aizaki, H.; Yoshida, A.; Deguchi, K.; Kumeta, M.; Junghof, J.; Wakita, T.; Takeyasu, K. Nanoimaging of Ssrna: Genome Architecture of the Hepatitis C Virus Revealed by Atomic Force Microscopy. *J. Nanomed. Nanotechnol.* **2014**, *S5*, 10.

(4) Segura-Ruiz, J.; Martínez-Criado, G.; Chu, M. H.; Denker, C.; Malindretos, J.; Rizzi, A. Synchrotron Nanoimaging of Single in-Rich Ingan Nanowires. *J. Appl. Phys.* **2013**, *113*, 136511.

(5) Amenabar, I.; Poly, S.; Goikoetxea, M.; Nuansing, W.; Lasch, P.; Hillenbrand, R. Hyperspectral Infrared Nanoimaging of Organic Samples Based on Fourier Transform Infrared Nanospectroscopy. *Nat. Commun.* **2017**, *8*, 14402.

(6) Chen, C.; Hayazawa, N.; Kawata, S. A 1.7 Nm Resolution Chemical Analysis of Carbon Nanotubes by Tip-Enhanced Raman Imaging in the Ambient. *Nat. Commun.* **2014**, *5*, 3312.

(7) Koshino, M.; Tanaka, T.; Solin, N.; Suenaga, K.; Isobe, H.; Nakamura, E. Imaging of Single Organic Molecules in Motion. *Science* **2007**, *316*, 853.

(8) Kusch, P.; Mastel, S.; Mueller, N. S.; Azpiazu, N. M.; Heeg, S.; Gorbachev, R.; Schedin, F.; Hübner, U.; Pascual, J. I.; Reich, S.; Hillenbrand, R. Dual-Scattering near-Field Microscope for Correlative Nanoimaging of Sers and Electromagnetic Hotspots. *Nano Lett.* **2017**, *17*, 2667−2673.

(9) Yeo, B.-S.; Stadler, J.; Schmid, T.; Zenobi, R.; Zhang, W. Tip-Enhanced Raman Spectroscopy—Its Status, Challenges and Future Directions. *Chem. Phys. Lett.* **2009**, *472*, 1−13.

(10) Deckert, V. Tip-Enhanced Raman Spectroscopy. *J. Raman Spectrosc.* **2009**, *40*, 1336−1337.

(11) Sonntag, M. D.; Pozzi, E. A.; Jiang, N.; Hersam, M. C.; Van Duyne, R. P. Recent Advances in Tip-Enhanced Raman Spectroscopy. *J. Phys. Chem. Lett.* **2014**, *5*, 3125−3130.

(12) Fang, Y.; Zhang, Z.; Sun, M. High Vacuum Tip-Enhanced Raman Spectroscope Based on a Scanning Tunneling Microscope. *Rev. Sci. Instrum.* **2016**, *87*, 033104.

(13) Zhang, Z.; Sheng, S.; Wang, R.; Sun, M. *Tip-Enhanced Raman Spectroscopy*; ACS Publications, 2016.

(14) Stöckle, R. M.; Suh, Y. D.; Deckert, V.; Zenobi, R. Nanoscale Chemical Analysis by Tip-Enhanced Raman Spectroscopy. *Chem. Phys. Lett.* **2000**, *318*, 131−136.

(15) Steidtner, J.; Pettinger, B. Tip-Enhanced Raman Spectroscopy and Microscopy on Single Dye Molecules with 15 Nm Resolution. *Phys. Rev. Lett.* **2008**, *100*, 236101.

(16) Zhang, R.; Zhang, Y.; Dong, Z. C.; Jiang, S.; Zhang, C.; Chen, L. G.; Zhang, L.; Liao, Y.; Aizpurua, J.; Luo, Y.; Yang, J. L.; Hou, J. G. Chemical Mapping of a Single Molecule by Plasmon-Enhanced Raman Scattering. *Nature* **2013**, *498*, 82−86.

(17) Liao, M.; Jiang, S.; Hu, C.; Zhang, R.; Kuang, Y.; Zhu, J.; Zhang, Y.; Dong, Z. Tip-Enhanced Raman Spectroscopic Imaging of

Individual Carbon Nanotubes with Subnanometer Resolution. *Nano Lett.* **2016**, *16*, 4040−4046.

(18) Bailo, E.; Deckert, V. Tip-Enhanced Raman Scattering. *Chem. Soc. Rev.* **2008**, *37*, 921−930.

(19) Deckert, V.; Zeisel, D.; Zenobi, R.; Vo-Dinh, T. Near-Field Surface-Enhanced Raman Imaging of Dye-Labeled DNA with 100-Nm Resolution. *Anal. Chem.* **1998**, *70*, 2646−2650.

(20) Deckert-Gaudig, T.; Deckert, V. Tip-Enhanced Raman Scattering Studies of Histidine on Novel Silver Substrates. *J. Raman Spectrosc.* **2009**, *40*, 1446−1451.

(21) Cançado, L. G.; Hartschuh, A.; Novotny, L. Tip-Enhanced Raman Spectroscopy of Carbon Nanotubes. *J. Raman Spectrosc.* **2009**, *40*, 1420−1426.

(22) Beams, R.; Cançado, L. G.; Jorio, A.; Vamivakas, A. N.; Novotny, L. Tip-Enhanced Raman Mapping of Local Strain in Graphene. *Nanotechnology* **2015**, *26*, 175702.

(23) Neacsu, C. C.; Dreyer, J.; Behr, N.; Raschke, M. B. Scanning-Probe Raman Spectroscopy with Single-Molecule Sensitivity. *Phys. Rev. B: Condens. Matter Mater. Phys.* **2006**, *73*, 193406.

(24) Wessel, J. Surface-Enhanced Optical Microscopy. *J. Opt. Soc. Am. B* **1985**, *2*, 1538−1541.

(25) Zhang, W.; Yeo, B. S.; Schmid, T.; Zenobi, R. Single Molecule Tip-Enhanced Raman Spectroscopy with Silver Tips. *J. Phys. Chem. C* **2007**, *111*, 1733−1738.

(26) Kusch, P.; Azpiazu, N. M.; Mueller, N. S.; Mastel, S.; Pascual, J. I.; Hillenbrand, R. Combined Tip-Enhanced Raman Spectroscopy and Scattering-Type Scanning near-Field Optical Microscopy. *J. Phys. Chem. C* **2018**, *122*, 16274.

(27) Vasconcelos, T. L.; Archanjo, B. S.; Fragneaud, B.; Oliveira, B. S.; Riikonen, J.; Li, C.; Ribeiro, D. S.; Rabelo, C.; Rodrigues, W. N.; Jorio, A.; Achete, C. A.; Cançado, L. G. Tuning Localized Surface Plasmon Resonance in Scanning near-Field Optical Microscopy Probes. *ACS Nano* **2015**, *9*, 6297−6304.

(28) Zhang, W.; Yeo, B.-S.; Schmid, T.; Hafner, C.; Zenobi, R. Nanoscale Roughness on Metal Surfaces Can Increase Tip-Enhanced Raman Scattering by an Order of Magnitude. *Nano Lett.* **2007**, *7*, 1401−1405.

(29) Stadler, J.; Oswald, B.; Schmid, T.; Zenobi, R. Characterizing Unusual Metal Substrates for Gap-Mode Tip-Enhanced Raman Spectroscopy. *J. Raman Spectrosc.* **2013**, *44*, 227−233.

(30) Alajlan, A. M.; Voronine, D. V.; Sinyukov, A. M.; Zhang, Z.; Sokolov, A. V.; Scully, M. O. Gap-Mode Enhancement on Mos2 Probed by Functionalized Tip-Enhanced Raman Spectroscopy. *Appl. Phys. Lett.* **2016**, *109*, 133106.

(31) Hartschuh, A.; Anderson, N.; Novotny, L. Near-Field Raman Spectroscopy Using a Sharp Metal Tip. *J. Microsc.* **2003**, *210*, 234−240.

(32) Asghari-Khiavi, M.; Wood, B. R.; Hojati-Talemi, P.; Downes, A.; McNaughton, D.; Mechler, A. Exploring the Origin of Tip-Enhanced Raman Scattering; Preparation of Efficient Ters Probes with High Yield. *J. Raman Spectrosc.* **2012**, *43*, 173−180.

(33) Ren, B.; Picardi, G.; Pettinger, B. Preparation of Gold Tips Suitable for Tip-Enhanced Raman Spectroscopy and Light Emission by Electrochemical Etching. *Rev. Sci. Instrum.* **2004**, *75*, 837−841.

(34) Yang, Z.; Aizpurua, J.; Xu, H. Electromagnetic Field Enhancement in Ters Configurations. *J. Raman Spectrosc.* **2009**, *40*, 1343−1348.

(35) Pettinger, B.; Ren, B.; Picardi, G.; Schuster, R.; Ertl, G. Nanoscale Probing of Adsorbed Species by Tip-Enhanced Raman Spectroscopy. *Phys. Rev. Lett.* **2004**, *92*, 096101.

(36) Guntherodt, G. *Light Scattering in Solids II*; Springer: Berlin/Heidelberg/New York, 1982.

(37) Kusch, P.; Breuer, S.; Ramsteiner, M.; Geelhaar, L.; Riechert, H.; Reich, S. Band Gap of Wurtzite Gaas: A Resonant Raman Study. *Phys. Rev. B: Condens. Matter Mater. Phys.* **2012**, *86*, 075317.

(38) Kusch, P.; Grelich, E.; Somaschini, C.; Luna, E.; Ramsteiner, M.; Geelhaar, L.; Riechert, H.; Reich, S. Type-Ii Band Alignment of Zinc-Blende and Wurtzite Segments in Gaas Nanowires: A Combined

Photoluminescence and Resonant Raman Scattering Study. *Phys. Rev. B: Condens. Matter Mater. Phys.* **2014**, *89*, 045310.

(39) Thomsen, C.; Reich, S. Double Resonant Raman Scattering in Graphite. *Phys. Rev. Lett.* **2000**, *85*, 5214−5217.

(40) Jorio, A.; Saito, R.; Hafner, J. H.; Lieber, C. M.; Hunter, M.; McClure, T.; Dresselhaus, G.; Dresselhaus, M. S. Structural (N, M) Determination of Isolated Single-Wall Carbon Nanotubes by Resonant Raman Scattering. *Phys. Rev. Lett.* **2001**, *86*, 1118−1121.

(41) Pettinger, B.; Ren, B.; Picardi, G.; Schuster, R.; Ertl, G. Tip-Enhanced Raman Spectroscopy (Ters) of Malachite Green Isothiocyanate at Au (111): Bleaching Behavior under the Influence of High Electromagnetic Fields. *J. Raman Spectrosc.* **2005**, *36*, 541−550.

(42) Schmitz, I.; Schreiner, M.; Friedbacher, G.; Grasserbauer, M. Tapping-Mode Afm in Comparison to Contact-Mode Afm as a Tool for in Situ Investigations of Surface Reactions with Reference to Glass Corrosion. *Anal. Chem.* **1997**, *69*, 1012−1018.

(43) Müssnich, L. C. P. A. M.; Chacham, H.; Soares, J. S.; Neto, N. M. B.; Shadmi, N.; Joselevich, E.; Cançado, L. G.; Jorio, A. Strain Discontinuity, Avalanche, and Memory in Carbon Nanotube Serpentine Systems. *Nano Lett.* **2015**, *15*, 5899−5904.

(44) Carozo, V.; Almeida, C. M.; Ferreira, E. H. M.; Cançado, L. G.; Achete, C. A.; Jorio, A. Raman Signature of Graphene Superlattices. *Nano Lett.* **2011**, *11*, 4527−4534.

(45) Bachilo, S. M.; Strano, M. S.; Kittrell, C.; Hauge, R. H.; Smalley, R. E.; Weisman, R. B. Structure-Assigned Optical Spectra of Single-Walled Carbon Nanotubes. *Science* **2002**, *298*, 2361−2366.

(46) Kataura, H.; Kumazawa, Y.; Maniwa, Y.; Umezu, I.; Suzuki, S.; Ohtsuka, Y.; Achiba, Y. Optical Properties of Single-Wall Carbon Nanotubes. *Synth. Met.* **1999**, *103*, 2555−2558.

(47) Johnson, P. B.; Christy, R. W. Optical Constants of the Noble Metals. *Phys. Rev. B: Solid State* **1972**, *6*, 4370−4379.

(48) Palik, E. D. *Handbook of Optical Constants of Solids*; Academic Press: London, 1998.

(49) Zhang, Z.; Chen, L.; Sun, M.; Ruan, P.; Zheng, H.; Xu, H. Insights into the Nature of Plasmon-Driven Catalytic Reactions Revealed by Hv-Ters. *Nanoscale* **2013**, *5*, 3249−3252.

(50) Le Ru, E.; Etchegoin, P. G. *Principle of Surface-Enhanced Raman Spectroscopy and Related Effects*; Elsevier: Amsterdam, 2009.

(51) Reich, S.; Thomsen, C.; Maultzsch, J. *Carbon Nanotubes: Basic Concepts and Physical Properties*; WILEY-VCH Verlag GmbH &Co. KGaA: Weinheim, 2004.

(52) Maultzsch, J.; Telg, H.; Reich, S.; Thomsen, C. Radial Breathing Mode of Single-Walled Carbon Nanotubes: Optical Transition Energies and Chiral-Index Assignment. *Phys. Rev. B: Condens. Matter Mater. Phys.* **2005**, *72*, 205438.

(53) Fantini, C.; Jorio, A.; Souza, M.; Strano, M. S.; Dresselhaus, M. S.; Pimenta, M. A. Optical Transition Energies for Carbon Nanotubes from Resonant Raman Spectroscopy: Environment and Temperature Effects. *Phys. Rev. Lett.* **2004**, *93*, 147406.

(54) Telg, H.; Maultzsch, J.; Reich, S.; Hennrich, F.; Thomsen, C. Chirality Distribution and Transition Energies of Carbon Nanotubes. *Phys. Rev. Lett.* **2004**, *93*, 177401.

(55) Telg, H.; Maultzsch, J.; Reich, S.; Thomsen, C. Resonant-Raman Intensities and Transition Energies of the E 11 Transition in Carbon Nanotubes. *Phys. Rev. B: Condens. Matter Mater. Phys.* **2006**, *74*, 115415.